

Smart Temperature Sensor Hot Water Cylinder Demand Management

Christian Struwig

Supervised by Alan Brent, Jonathan Zukerman, and Daniel Burmester.

Abstract—The goal of Aotearoa having 100% of its energy from renewable sources urges for the improvement of existing demand management technologies. Existing technologies like Ripple Control, externally controls residential electric hot water cylinders to help manage demand, however, its use has declined rapidly in recent times. This paper presents and evaluates an affordable alternative hot water controller by using an energy harvesting Internet of Things smart temperature sensor found at the outlet pipe of a hot water cylinder. The smart temperature sensor is charged by harvesting the thermal energy from the temperature gradient between the outlet pipe and the ambient air using mounted Thermoelectric generator (TEG) modules. Using Bluetooth Low-Energy the smart temperature sensor relays accurate temperature readings of the stored hot water. The power electronic interface of the TEG module is a low-power DC-DC boost converter that charges a lithium-ion battery. The estimated energy consumption is simulated and used for the design and development of the device. The expected energy consumption is later evaluated with the recorded consumption. Thermal data gathered from an electric hot water cylinder and thermal modelling software is used to evaluate the performance of the TEG modules to be selected to meet the energy demands of the smart temperature sensor. The boost converter design is simulated and developed. The real performance of the boost converter and TEG modules are then tested and compared with the simulated results. The paper investigates battery lifetime, transmission range and the boost converter performance of the smart temperature sensor. A final cost evaluation is also performed on the smart temperature sensor. It is found that the controller is technically and economically viable in Aotearoa.

I. INTRODUCTION

A. Big Picture

In Aotearoa, as of 2022, 87% of electricity generation was from renewable energy systems primarily hydro, geothermal and wind [1]. Twenty percent of this renewable energy growth occurred in the past decade, and it is aimed to achieve 100% renewable electricity by 2030 [1]. The New Zealand government's clean vehicle discount has led to the uptake of electric vehicles and vehicle charging [2], [3]. The increased growth of charging raises concern about the potential impact on Aotearoa's low-voltage network but also presents an opportunity with its ability to be remotely managed. A New Zealand case study pointed out a potential national-level generation shortage based on future EV uptake [4]. This was due to the EV charging loads coinciding with residential loads which increases peak demand. This would require future reduction strategies such as adopting new technology and bettering demand management [1], [5].

B. The Problem

For New Zealand's energy to be 100% renewable, much will need to come from intermittent generation types, specifically solar and wind. To account for cloudy or calm days, the options are limited to overbuilding of generation, energy storage or demand management.

Demand management or demand response focuses on the reduction of power consumption to ensure improved grid stability (by matching demand to available generation), to ensure the integrity of electricity network assets and also reduce a client's electricity tariffs [6]. Ripple control is a form of demand management technology that enables the external control of electricity consumers' hot water cylinders, which is limited to switching it on and off [7].

Looking at Aotearoa's residential demand side, one-third of household electricity is occupied by electric hot water cylinders [1]. Ripple control benefits consumers as it lowers expenditure on grid upgrades which ultimately maintains low tariffs. It also benefits distribution businesses as it lowers their transmission costs from the grid owner, Transpower [7]. The Energy Efficiency & Conservation Authority, however, estimated that less than half of the residential electricity consumers made use of ripple control [7]. The leading causes are the cost of residential ripple control relays which is around \$300 per control point and the independent external control of hot water cylinders.

C. Objective

The objective is to develop a smart temperature sensor that is to be mounted onto the outlet pipe of a hot water cylinder, Fig. 1. The smart temperature sensor wirelessly relays the temperature measured at the outlet pipe to provide an approximate temperature of the hot water stored inside the hot water cylinder. The relayed temperature is to be received by a hot water controller, that adjusts the power fed to the hot water cylinder which is not part of the project deliverable.

The smart temperature sensor is aimed as an alternate demand management technology that is to be an addition to Thundergrid's dynamic load management EV charger network. The smart temperature sensor therefore provides the ability to manage hot water cylinders remotely through Thundergrid's cloud-based technology that would supersede existing ripple control technology. It would allow for the dynamic control of hot water cylinders to provide additional flexibility in demand management and lower the cost of grid upgrades which benefits the grid owner. Customers also benefit by being

able to control when their hot water cylinders are active and reject grid owner requests to disable their hot water cylinders.

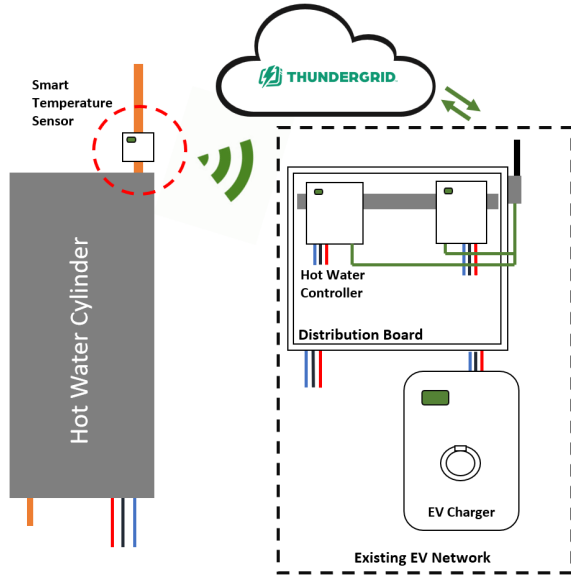


Fig. 1. Sketch of the Smart Temperature Sensor involvement in the hot water controller system.

D. Deliverable

A smart temperature sensor mounted at the outlet pipe of a hot water cylinder is to be developed. It is required to relay the temperature of the outlet pipe wirelessly with readings close to 5% of the true temperature. The wireless transmission must have a minimum range of 30 meters to successfully reach the building's distribution board. It is aimed to be a low-power Internet of Things, or IOT, device that mounts onto the outlet pipe with minimal effort and must not be connected to a building's existing electrics. It is therefore required to be self-powered either through batteries or by surrounding available energy sources and must last for longer than 6 months. The smart temperature sensor is also expected to not cost more than existing ripple control relays.

II. RELATED WORK

Research into related solutions and associated technologies has been conducted to assist in the design and implementation of the smart temperature sensor. The associated technologies for the smart temperature sensor were thermoelectric generators and IOT devices.

A. Thermoelectric Generators

A thermoelectric generator (TEG) module could be a potential power source utilised by the smart temperature sensor that makes use of the available thermal energy from the outlet pipe. The TEG module functions on the Seebeck Effect to convert thermal energy into electrical energy [8], [9].

From Fig. 2, it is comprised of numerous thermopiles or thermoelements, which are groups of connected thermocouples [9]. The thermocouples are electrically connected in series and

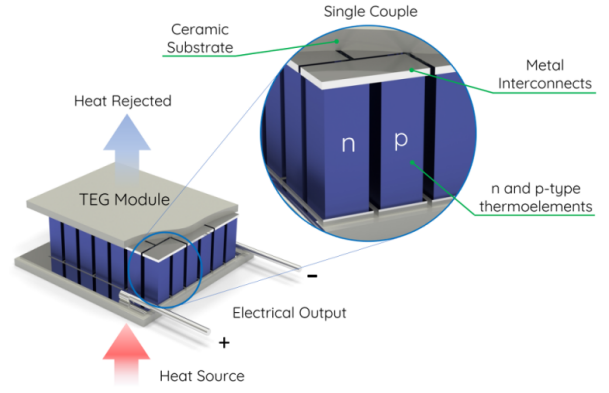


Fig. 2. Breakdown of Thermoelectric Generator Module, Source: Adapted from [12]

thermally connected in parallel. The voltage across the TEG module can be expressed with equation (1) [10].

$$V_{out} = \alpha_{TEG} \Delta T \quad [V] \quad (1)$$

Where ΔT is the temperature gradient and α_{TEG} is the Seebeck coefficient of the TEG module [10].

The voltage can be increased by increasing the number of series-connected TEG modules [10]. This however will increase the internal resistance and reduce the total power output (2).

$$P = \frac{V_{out}^2 R_L}{(R_{TEG} + R_L)^2} \quad [W] \quad (2)$$

Where R_L is the load resistance and R_{TEG} is the TEG module resistance. Increasing the temperature gradient can also increase the voltage output of the TEG module, however, this is dependent on the type of environment the TEG is situated in [10].

The thermoelectric performance of TEG modules can be characterized by their Seebeck coefficient for peak thermal to electrical energy conversion, electrical conductivity to reduce the internal resistance and thermal conduction to determine the amount of heat conducting through the TEG module [9]–[11].

This can all be summarized by the figure of merit, ZT or ZT -metric (3).

$$ZT = \frac{\alpha^2}{\rho k} T \quad (3)$$

Where α is the Seebeck coefficient, ρ is electrical resistivity, k is the thermal conductance and T is the absolute temperature [9]–[11]. The greater the ZT metric, the better the thermoelectric performance of the TEG module.

B. Related Solutions

The smart temperature sensor is an IOT-based device. Internet of Things or IOT are embedded devices that share their data through a network [13]. This section reviewed related low-power IOT solutions that involve temperature sensing and control. This aided in the selection of suitable low-power network protocols and design of the smart temperature sensor.

A design was proposed for an IOT-based "infant incubator" monitoring system that used a microcontroller, data acquisition module and data communication sub-module [13]. The design used an Arduino Uno Rev3 microcontroller that interfaced with an ESP8266 Wi-Fi module that outputs readings from an LM35 IC temperature sensor. The system made use of additional sensors, which pushed the use of the Arduino as it contained fourteen digital and six analogue pins. The choice of LM35 was selected due to its reduced external circuitry, good linearity, and its low current draw of 60 micro amperes [13]. The design report indicated anomaly temperature readings; however, this was due to the LM35 not being a wearable sensor, yet it still provided accurate readings with a 1% error. This report had not covered the system's power consumption, especially concerning the current draw experienced at transmitting and receiving data from the ESP8266 Wi-Fi module.

A real-time data acquisition system was developed for control purposes with the use of Zigbee network protocols and Arduino [14]. The DHT22 sensor was used, which has an accuracy of $\pm 0.5^{\circ}\text{C}$ and a range of -40°C to $+125^{\circ}\text{C}$. The system used Xbee S2C modules that support Zigbee protocol with a 1200m range at 250Kbps. The modules are programmable microcontrollers that possess several digital and analogue pins that provide serial communication. The Zigbee protocol was used in Transparent Mode, which is a unique mode that transmits data without alteration as if it were over a serial line [14]. The Transparent Mode is well suited for establishing between two devices without the need for new connections to the Zigbee network.

Trakya University in Turkey developed a Bluetooth Low Energy sensor node for precision agricultural practices [15]. The research focused on the power consumption and management cost of the nodes. The nodes consisted of a Texas Instruments CC2541 Bluetooth system on a chip, or SoC, that connected to an MCP9808 temperature sensor and BH1750FVI ambient light sensor. The CC2541 SoC has a 2.4GHz RF transceiver, 8051 microcontroller, 8KB Ram and a range of available peripherals. The entire node was powered by a single 3V cr2032 Li-Mn battery [15]. The nodes periodically went into a sleep state for 1 minute which consumed 0.0025mA and 13.84mA during the awake state for 3.2ms. The average power consumption of the nodes where $3.2\mu\text{A}$ which amounted to 71317.82 hours using the 230mAh cr2032 battery [15]. With the inclusion of a BLE gateway to communicate with the entire sensor module, it was found to cost the agriculture sector under \$500 a year per 1 hectare.

A paper reported on wireless sensor nodes for environmental monitoring using IOT [16]. These nodes were powered through energy harvesting modules that relayed environmental parameters such as temperature and acoustic noise utilizing Bluetooth low-energy transceivers. The energy harvesting modules gathered energy from multiple sources such as radio waves, solar and wireless power transmission [16]. The energy storage was implemented through a supercapacitor, with an RF energy collection frequency range of 915-1550MHz and solar energy harvested from a 5x20cm² solar panel. The temperature sensor in the node was an MCP9700 IC with a sensing range of -40°C to $+125^{\circ}\text{C}$. A nRF51822 SoC was

used which supported Bluetooth low energy protocol [16]. The power consumption was reduced by reducing the transmission power and decreasing the advertising time of the BLE module in the SoC. The power consumption during sleep was $0.4\mu\text{A}$ and $2.3\mu\text{A}$ during on state.

III. DESIGN

A. Design Requirements

The smart temperature sensor to be designed was expected to operate independently with minimal installation effort. It therefore required to be self-powered either through battery storage or other available sources such as thermal energy. For seamless integration with the existing hot water cylinder wiring, it needed to transmit its readings wirelessly to the hot water controller by using a low-power network protocol. The temperature readings at the outlet pipe were required to be accurate to help provide a good estimate of the water temperature inside the hot water cylinder. It was expected to function at an average internal temperature of 50°C surrounded by an ambient temperature of 20°C .

The system design needed to prioritise lifetime, current consumption, efficiency, sampling frequency and cost. A well-designed system was expected not to cost more than the currently available ripple control devices. The smart temperature sensor must have had a minimum lifetime of 6 months and must achieve water temperature readings that were within 5% of the actual water temperature. Striking a balance between the sampling frequency and the current consumption was key as it drove data collection quality and device lifetime.

B. Hot Water Cylinder Data

In assistance with driving the system design and implementation, preliminary data was gathered on a 225-litre Rheem cylinder that operated at 8.5A 230V AC. The following data was taken:

- Temperature on the outlet pipe
- Ambient temperature around the outlet pipe
- Temperature at the Thermostat probe point
- Current draw of the Thermostat

The preliminary data assisted in understanding the operation of an electric hot water cylinder, finding the available thermal energy for harvesting, calculating the expected output performance of thermoelectric generator modules and determining a suitable sampling rate.

From Fig. 3, the outer outlet pipe temperature averaged at 50.4°C while the average thermostat temperature was 59.2°C . This indicated an average temperature gradient of 10°C between the inner and outer pipe temperature. The temperature drops rapidly at the thermostat when hot water is drawn, as hot water flows out of the cylinder and through the copper pipe which relates to the 5°C spike. Closing the tap, traps hot water in the pipe, which is no longer thermally insulated. This drives the trapped heat energy to flow through the pipe sides and out to the ambient air using conduction and convective heat transfer, which relates to the steady decline back to 50°C after the spike.

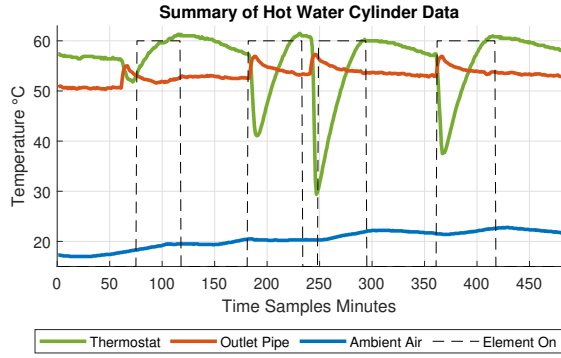


Fig. 3. Summary of Hot Water Cylinder Data recorded from 8am-4pm every minute

$$Q' = \frac{kA\Delta T}{D} = \frac{2\pi Lk\Delta T}{\ln\left(\frac{R_o}{R_i}\right)} \quad [W] \quad (4)$$

Using the average temperature gradient, 10°C , and the thermal conductivity for copper, $390 \text{ W m}^{-1} \text{ K}^{-1}$, the rate of available heat flow was found by using Fourier's equation for heat conduction (4). Using the New Zealand Standard 3501 for pipe dimensions, measuring a 14mm outer radius with an expected 13.4mm inner radius, the total heat transfer was 83kW at 150cm pipe length [17]. This indicated that there was 1079 W m^{-2} of available thermal power that could be used by the smart temperature sensor employing the Seebeck Effect [10].

C. Thermoelectric Requirements and Calculations

Thermoelectric Generators or TEGs were required to make use of the available thermal energy and corresponding electrical energy from the Seebeck Effect to power the smart temperature sensor. Fig. 2 highlights that TEGs are designed as flat modules with corresponding hot and cold sides. This created a challenge in design as the hot side of the TEG module was a 28mm diameter cylinder.

TEG modules with dimensions smaller or equal to the 28mm diameter was therefore needed to allow for multiple modules to be mounted around the pipe for maximum surface contact which correlated to increased thermal energy harvesting. The modules however still required a thermal interface, such as a copper block with a convex side, to ensure that the entire face of the hot side made contact with the copper pipe. Table 1 shows the list of possible TEG modules that were able to meet the design constraint with their respective summarised performances from datasheets [18]–[21].

In Table 2, the expected performance and respective Seebeck coefficients of the modules on the outlet pipe were calculated by using their performance values (1). Assuming an average temperature gradient, between the outer pipe and the ambient air, of 32.85°C ; the expected open circuit output voltage of the modules was also found (1). The expected maximum achievable efficiency of the modules was calculated by using their listed ZT-metric (5).

TABLE I
DATASHEET PERFORMANCE OF SUITABLE MODULES ($\Delta T = 28^\circ\text{C}$)
[18]–[21]

Module	RC3-2.5	RC3-4.5	NL1023T	RC6-4
Length mm	20.5	20.5	13.16	28
Width mm	16	16	13.16	23.5
OC Voltage mV	370	370	850	840
SC Current mA	270	410	190	400
Optimum Voltage mV	210	208	482	475
Cost \$	38.01	32.5	34.2	38.14
Resistance $^\circ\text{C W}^{-1}$	14.46	9.54	9.09	4.19
Device ZT	0.76	0.74	0.77	0.74

$$\eta_{max} = \frac{T_h - T_c}{T_h} \frac{(\sqrt{1 + ZT} - 1)}{\sqrt{1 + ZT} + \frac{T_c}{T_h}} \quad (5)$$

The amount of heat flow required to achieve the calculated open circuit voltage of the modules was also calculated by using their respective thermal resistances (6).

$$Q' = \frac{\Delta T}{R_{th}} \quad [W] \quad (6)$$

In Table 2, the clear option was the NL1023T module. It provided the highest efficiency and a high output voltage for the amount of heat flow required. This however was the open circuit voltage and does not accurately reflect the input voltage to the temperature sensor. This was about the concept of load matching, where the internal resistance of the module is lower than the expected load of the temperature sensor which would reduce the total power output (2).

TABLE II
CALCULATED PERFORMANCE OF SUITABLE MODULES ($\Delta T = 32.85^\circ\text{C}$)

Module	RC3-2.5	RC3-4.5	NL1023T	RC6-4
Seebeck Coef. α	0.0132	0.0132	0.0303	0.03
OC Voltage mV	434	434	997	985
Max Efficiency %	9.1	9.0	9.2	8.6
Heat Flow Q' W	2.3	3.5	3.67	7.97

A better output voltage calculation was using the module's optimum output voltage from the datasheet for maximum efficiency. Using the module's optimum voltage of 482mV in Fig. 4; provided a calculated output voltage of 565mV at the outlet pipe.

D. Heat Sink Design

The second challenge was ensuring that the cold side of the modules remained at a lower temperature. The cold side temperature would increase over time due to the module's intrinsic self-heating characteristics [11]. This led to a maximum cold side constraint of 30°C under the assumption of having 20°C ambient temperature. A suitable heat sink was the only option as the available cold source was limited to the ambient air surrounding the pipe. Forced convection, such as a fan, was not an available design option as the majority of the power produced by the module would be wasted on the fan.

A thermal resistance circuit, Fig. 5, was drawn up to assist in calculating the required heat sink for the TEG module where

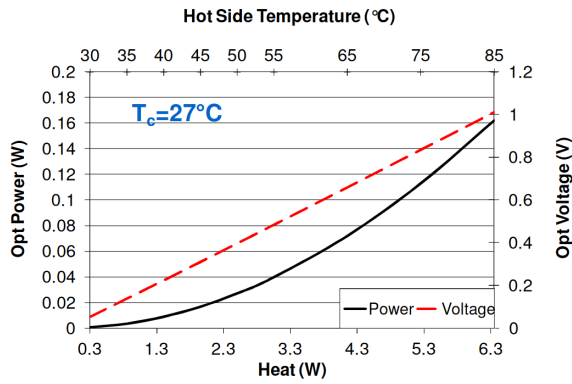


Fig. 4. NL1023T datasheet performance curve, Optimum Voltage and Power vs Heat. Source: Taken from

the resistance of the thermal interface, the R_{block} , between the pipe and module was small and can be ignored. The rated thermal resistance of $9.09^{\circ}\text{C}/\text{W}$ was used for the TEG module [21]. Assuming a minimum 30°C cold side temperature, the total power dissipated through the module was calculated to be 2.2W (6).

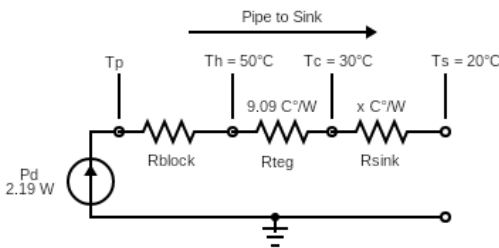


Fig. 5. Thermal resistance circuit showing heat dissipated across the expected thermal resistances.

The minimum heat sink thermal resistance required to meet that same power dissipation was calculated to be $4.5^{\circ}\text{C}/\text{W}$, at an assumed ambient temperature of 20°C (7).

$$R_{total} = R_{teg} + R_{sink} = \frac{\Delta T_{total}}{P_d} \quad [^{\circ}\text{C}/\text{W}] \quad (7)$$

A heat sink that could draw the desired 3.6W instead of 2.2W heat across the module whilst being smaller than 28mm was not achievable. At 3.6W the cold side temperature required would be 17.3°C , which was below the average ambient temperature of 20°C .

E. System Design

The smart temperature sensor was designed to be mounted onto the outlet pipe of the hot water cylinder. This required a mounting bracket that allowed for the TEG modules to be clamped around the pipe and have direct thermal contact for maximum heat transfer. The bracket needed to support the rest of the system namely the low-power microcontroller, network protocol module, temperature sensor and battery storage. The bracket material was important, as it impacted the performance

of the modules. Insulating materials such as high-temperature plastics had the possibility of insulating the heat on the copper pipe and redirecting the heat flow through the modules increasing performance.

Adhering to the design requirements, the design featured a rechargeable battery storage system that supported the smart temperature sensor for 1 year. A battery system supporting a network protocol module and microcontroller led to a operating voltage of 3V .

Therefore, a series of modules were required to exceed the 3V threshold for battery charging. A collection of modules was too expensive which led to the need for a DC-DC boost converter, that stepped up the $100\text{-}500\text{mV}$ module output to a constant 3V output.

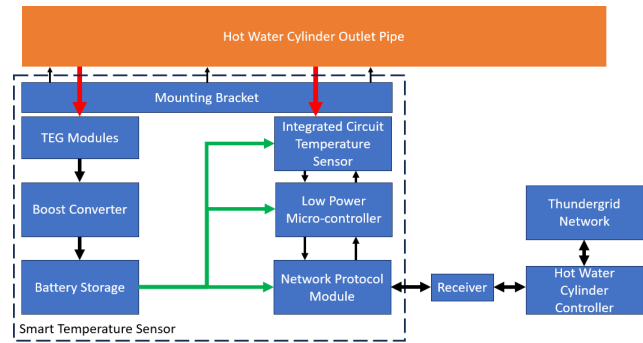


Fig. 6. Block diagram of the smart temperature sensor design

A low-power microcontroller that operated at 3V was needed to store and transmit temperature readings. The controller allowed for low-power functionality that reduced current consumption to microamps by disabling the integrated temperature sensor and network protocol module between samples. In low-power mode, the controller only consumed enough current to run a watchdog timer that kept track of the sample interval.

An integrated circuit or IC temperature sensor was implemented for the design. The smaller circuitry, a single bipolar transistor, with the associated reduced current consumption aligned with the design requirements. The accurate digital output of the sensor eliminated the need for analog to digital circuitry and was fed directly to the microcontroller.

A low-power network module was added to the design for wireless communication with the receiver on the hot water cylinder controller. The network module used a protocol such as Bluetooth Low Energy, Zigbee or Wi-Fi for a proximity range of 10 meters. The protocol that had the lowest current consumption was needed to prolong battery life.

From Fig. 6, the flow chart shows the operational flow of the smart temperature sensor. The watchdog timer of the microcontroller was used to keep track of the low-power state. When it timed out, it created a reset operation which forced the microcontroller to turn on.

The microcontroller would enable the network module and the IC temperature sensor. The network module advertised its connection availability and the hot water cylinder controller's receiver connected.

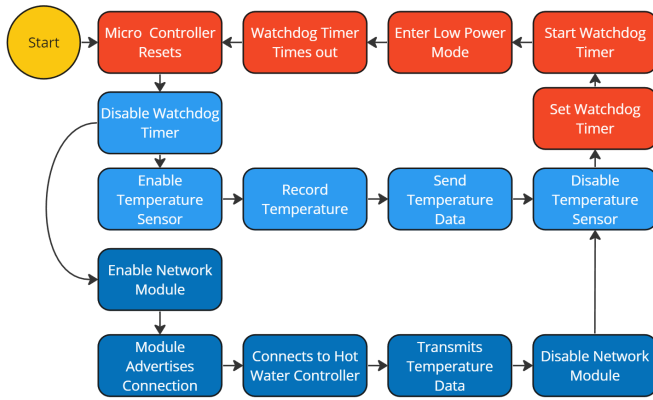


Fig. 7. Flow chart of the smart temperature sensor operation

A temperature read request was sent to the IC temperature sensor from the controller. The IC temperature sensor read the temperature at the outlet pipe, and returned the value to the controller. The temperature recording was then transmitted to the receiver of the hot water controller. After transmission, the network module and IC temperature sensor were disabled by the controller. The controller reprogrammed and started the watchdog timer before it entered low-power mode.

IV. IMPLEMENTATION

A. Component Selection

1) *Microcontroller*: The microcontroller selected is the AT-TINY 85, a low-power 3V 8-bit controller designed for IOT devices [22]. It has a rated low current consumption of 300 μ A at active mode and 0.1 μ A at sleep mode. Meeting design requirements, it has a programmable watchdog timer and 8 programmable output lines that are used to communicate with and disable the network module and IC temperature sensor [22].

2) *IC Temperature Sensor*: The DS18B20 digital temperature sensor was selected. It has a measuring range of -55 $^{\circ}$ C to +125 $^{\circ}$ C with a 9-bit to 12-bit configurable resolution [23]. It is rated to measure temperatures within 0.0625 $^{\circ}$ C at its highest resolution. The sensor communicates via 1-Wire bus protocol and only needs a single connection with the microcontroller to communicate. Operating at 3V, it has a rated consumption of 1000nA during idle mode and 1.5mA during sense requests [23].

3) *Network Module*: The BLE HM-10 network module was selected, which operates on the Bluetooth Specification V4.0 low energy network protocol [24]. It has a working frequency of 2.4GHz which correlates to a maximum transmission range of 30 meters which met the design requirements. At 3V operation, the module has a rated current consumption of 200 μ A during sleep and 15mA during transmission [24]. The module communicates with the microcontroller via a 2-wire universal asynchronous receiver transmitter, UART, communication protocol.

B. Current Consumption and Battery Selection

The lifetime and operation of the smart temperature sensor was dependent on the average current consumption and the

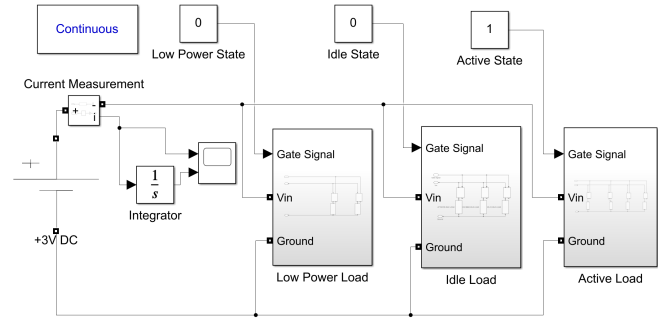


Fig. 8. Matlab Simulink model of load sub-circuits determined the current draw from operation states

battery capacity of the system. From Fig. 8, a Simulink model was created to assist in evaluating the expected current consumption by using the datasheet resistance values of the selected components. The model was based on three expected operation states namely active, idle and sleep. The current consumption was found for each of the three states of operation by having 3 separate load sub-circuits, which were based on the rated current values for each component at the respective operating state.

The current consumption was found to be 0.732mA, 8.21mA, 16.7mA for sleep, idle and active states. The use of only active current was not an accurate reflection of the overall current consumption, as the device spends most of its time in the sleep state. The average current was taken instead which is the sum of time spent at each current draw divided by the total time, where the total time is the sampling rate (8). An extreme assumption is used, where it is in the active state for 2 seconds and 1 second in idle state during samples.

$$\bar{I} = \frac{\sum t_{state} \times I_{state}}{Total\ Time} \quad [mA] \quad (8)$$

Fig. 9 shows the expected average current consumption in terms of sampling rate. The average current consumption was used to determine the battery lifetime from the rated battery capacities of rechargeable 3V batteries. None of the listed battery types lasted more than 6 months, due to the high sleep state current consumption. This required additional circuit optimisation methods to further reduce sleep state current consumption.

The 3.7V 18650 battery was chosen as it provides the longest lifetime of 91 days. This requires that the boost converter outputs a voltage of 4.1V to successfully charge the battery.

From Fig.10 and Fig.9, the reduction of the sampling rate lowered the average current however it also reduced data quality. This caused the temperature sensor to inaccurately capture the outlet pipe temperature curve especially when hot water was drawn. It was therefore recommended that the minimum sample rate was no more than 5 minutes.

C. Boost Converter Circuit

The designed boost converter had an input voltage requirement range of 100-500mV to 4.2V output. The output voltage

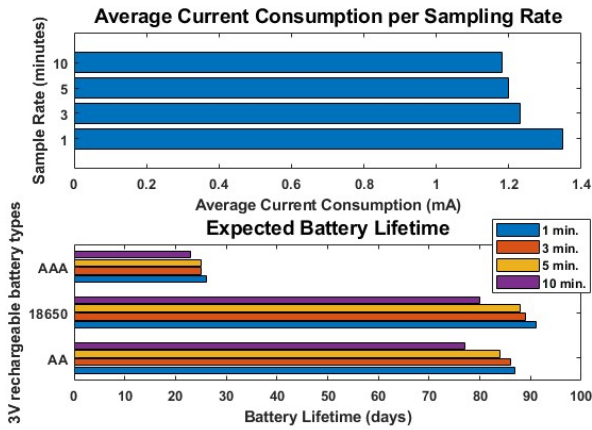


Fig. 9. Average Current Consumption and Battery Lifetime

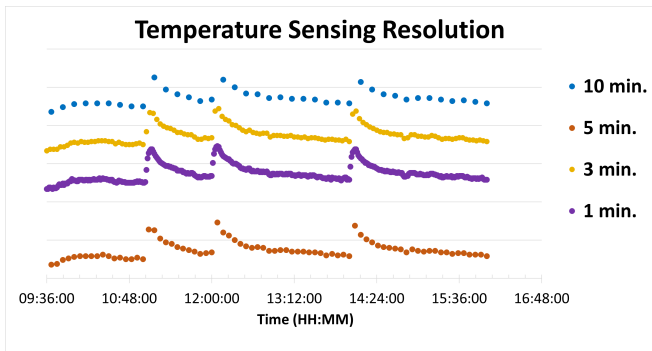


Fig. 10. Data resolution reduced as the sample rate lowered.

was required not to exceed the charge voltage to prevent overcharge damage of the Li-ion battery. This adhered to the concept of float voltage which was the maintained voltage after a complete charge. This ensured to keep the battery capacity at maintenance by compensating for battery self-discharge. The float voltage was required to decrease for the rise in temperatures exceeding 50°C, to prevent overcharge damage.

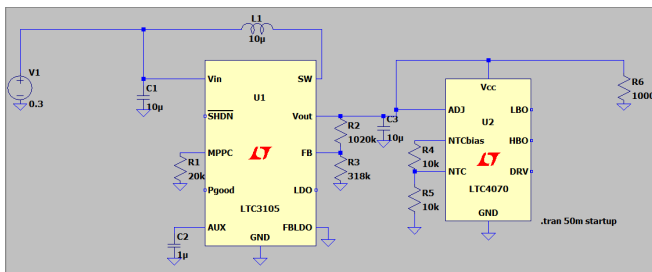


Fig. 11. Circuit Schematic of LtSpice Simulation Boost Converter

The boost converter requirements led to the selection of the LTC3105 step-up converter, Fig.11, designed for low voltage energy harvesting applications such as TEG modules and photovoltaic cells [25]. It operated at minimum input voltage of 225mV for an output voltage range of 1.6V to 5.2V [25]. The required 4.2V output voltage was configured by adjusting the voltage divider circuit between the V_{OUT} and FB pins, where FB was the feedback input to the boost converter using

equation (9).

$$V_{out} = 1.004 \times \left(\frac{R2}{R3} + 1 \right) \quad [V] \quad (9)$$

The ability to boost low voltages to 4.1V was achieved by the LTC3105 making use of a 1μF capacitor at V_{AUX} that charged up to 1.4V [25]. From Fig. 12, it charged AUX and the LDO pins until AUX was higher than the regulated voltage of LDO, where the excess charge was transferred to V_{OUT} for charging. An internal switch connected V_{OUT} to AUX when the former exceeds the latter at 2.6V where the V_{OUT} pin rose to 4.1V after 5ms [25]. The boost converter then went into normal operation, using the input inductor’s stored energy to supply the higher voltage.

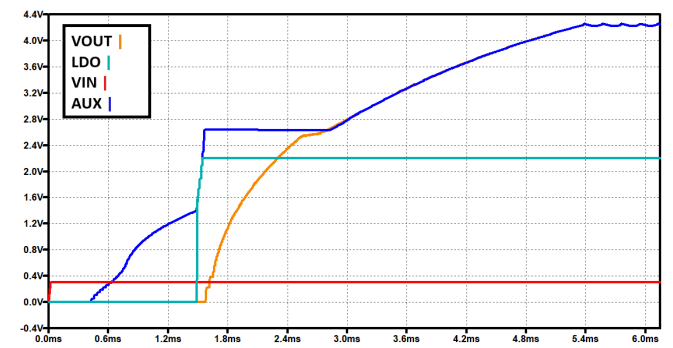


Fig. 12. Output Curve of LtSpice Simulation Boost Converter showing V_{OUT}, AUX, LDO and V_{IN}.

A low DC resistance 10μH input inductor was chosen to ensure higher efficiency and a low start-up voltage. The LTC3105 also offered maximum power point control, MPPC, that adjusted the inductor current to set the input voltage to a desired value for maximum power input [25]. The input voltage was configured to 300mV with a 30kΩ resistor that tied MPPC to ground, where the assumed output from the TEG modules were 300mV.

Attached to the output of the LTC3105 was the LTC4070 Li-Ion shunt battery charger system designed for energy harvesting applications [26]. It provided the ability to charge Li-ion batteries at low currents, 450nA, from intermittent output sources such as the TEG modules. As the battery voltage approached the float voltage, it would shunt the current away from the battery, which reduced the charging current [26].

Low current output from the boost converter was expected, due to boosted voltage conversely lowered the output current. The LTC4070 lowered the battery float voltage accordingly when temperatures exceeded 40°C with the use of a 10kΩ thermistor voltage divider [26].

From Fig. 11 and Fig. 12, the LTC3105 and LTC4070 were first simulated in LtSpice simulation software to ensure that the boost converter circuit was operational before the physical implementation.

D. Temperature Sensor Circuit

The temperature sensor circuit was designed by using the selected components. From Fig. 13, the microcontroller’s general

purpose pins were used to connect the HM-10 network module as a two-wire UART protocol with BLE_TX and BLE_RX [24]. The DS18B20 IC temperature sensor was also connected to the microcontroller with the 1-Wire line [23]. The circuit assumed an input voltage of 3.3V for components however, it also worked with 3.7V input from the 18650 battery.

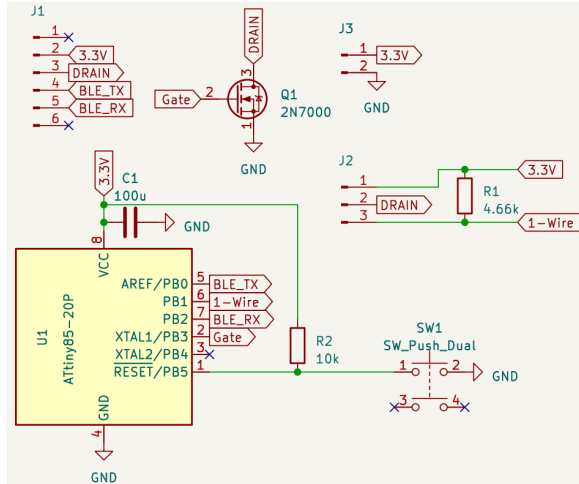


Fig. 13. Circuit Schematic of the Temperature Sensor Circuit

The RESET pin on the microcontroller was utilised with a push pin switch, where the controller restarted when the reset pin was pulled low [22]. The undesirable 700mA during sleep state was reduced by the implementation of a 2N7000 N-Channel MOSFET disabled the HM-10 network module and the DS18B20 temperature sensor [23], [24]. The microcontroller handled the gate of the MOSFET which reduced the sleep state current to only 10µA which came from the microcontroller.

E. Full System Implementation

1) *Thermal Block*: A 14mmx14mm thermal block was machined that acted as the thermal interface between the pipe and the TEG Modules. Aluminium was used to provide high thermal conduction to the hot side of the TEG module. The thermal block's curved side ensures that the entire face of the TEG module makes contact with the pipe.

2) *Mounting Bracket*: The mounting bracket design has a square extruded cut in the center, pictured in Fig. 14 and 15, which holds the thermal block and TEG modules in place which was printed with ABS plastic. It was selected for its high melting temperature of 245°C and high tensile strength of 44N/mm² that ensured a long operational lifetime on the 50°C pipe [27]. The design allows for two TEG modules to be connected underneath each other. This provided the flexibility of additional TEG modules which could be connected in series for increased power input to the boost converter.

3) *Mounting Platform*: The mounting platform, seen in Fig. 14 and 15, was created to allow for the battery, boost converter and temperature sensor circuits to be mounted onto the bracket. It was made as a printed circuit board so that the wires from the TEG modules were soldered onto the board which ensured a firm connection to the boost converter. As seen in Fig. 15, a

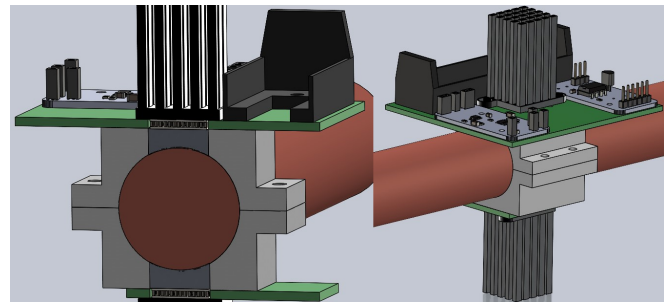


Fig. 14. Modeled SolidWorks design of the entire system

smaller mounting platform was created for the additional TEG modules. The smaller mounting platform and the mounting bracket were modular, therefore one could stack more TEG modules in series along the outlet pipe if desired.

4) *Heat Sink*: The 19mmx19mm Wakefield Aluminium heat sink was selected for cooling the TEG modules [28]. The heat sink provides a thermal resistance of 3.7°C/W at 33mm fin height which is under the 4.5°C/W design requirement [28]. The small form factor is under the 28mm requirement which makes it light enough to be attached to the mounting platform. The plastic spring push-pin variant was selected as the spring pushes the heat sink into the platform and bracket [28]. This ensures a firm connection between the TEG modules and the heat sink and that of the thermal block and TEG modules.

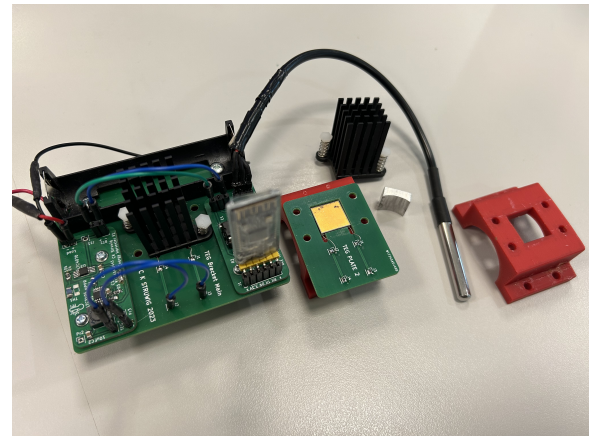


Fig. 15. Image of the implemented Smart Temperature Sensor with the addition of a heat sink removed to show the TEG module inside the bracket.

5) *Thermal Conduction Analysis*: A thermal conduction analysis was performed on a modelled SolidWorks system that verified if the design provided a suitable temperature difference across the TEG module.

The thermal analysis assumed an ambient air temperature of 20°C with a convection coefficient of 25W/(m² K) around the heat sink. A thermal resistance of 0.001 (K m²)/W was specified between the touching components which prevented heat from transferring perfectly between them. From Fig. 16, the design produced an adequate temperature gradient of 26°C across the TEG module, which was expected to produce a voltage of 380mV (1).

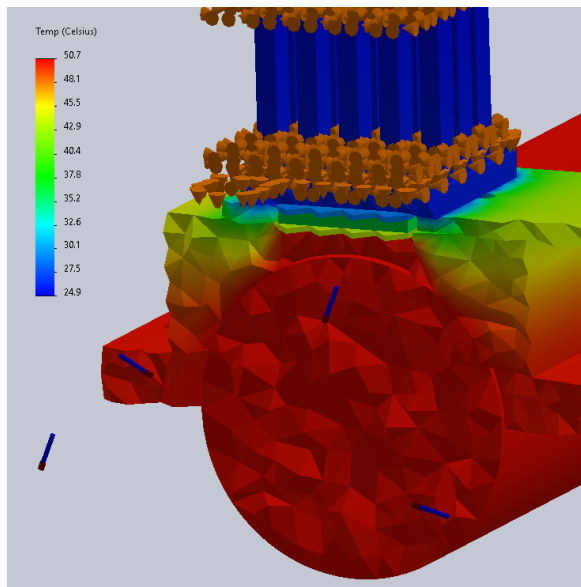


Fig. 16. Thermal section view of the modelled system

V. EVALUATION

The evaluation was concerned with the smart temperature sensor’s current consumption, the output performance of the TEG module, the boost converter efficiency, the battery charge rate and the cost that was compared to the estimated design calculations and the existing ripple control relay.

A. Power Consumption

The power consumption of the system was evaluated in terms of the recorded current consumption at the idle, sleep and on states by the temperature sensor circuit. The operation was also seen by plotting the current draw curve of the system. Using the found values, the battery lifetime and total on time was determined. The evaluation expanded to the performance of the network module’s transmission range and the performance benefit of using a switched MOSFET to disable the module network during sleep states.

Fig. 16 shows the current curve of the smart temperature sensor at 3.3V input voltage which was recorded with a current data logger at the input point of the temperature sensor. It had a 13mA current draw during the 0.7s on state. The majority of time went to microcontroller operation and lesser so to reading operation and wireless transmission of the temperature, Fig. 20.

The current draw during the idle state was 3mA, which was due to the fixed 0.5s operation of the watchdog timer before entering sleep mode. The watchdog timer had a maximum programmable time of 8 seconds which had to be reset continuously, as seen at the 14s mark in Fig. 17, until the total overlapped time was equal to the sampling time at 17.5s [22].

The recorded average current draw during sleep state was 4.75µA which was significantly lower than the simulated current draw of 700µA.

The average current consumption and battery life were recalculated using the measured current found in the sleep, idle

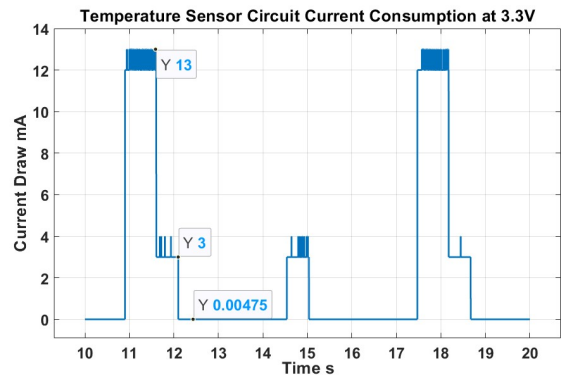


Fig. 17. Temperature sensor circuit current curve, showing the sleep, idle and on states.

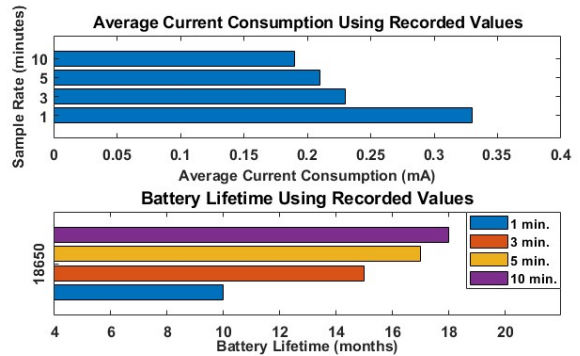


Fig. 18. Recalculated average current consumption and battery lifetime using the measured current during sleep, idle and on states.

and on states, as seen in Fig. 18. The minimum battery lifetime at 1-minute sample rate was 10 months, which increased to 18 months using a 10-minute sample rate. This was significantly greater than the simulated maximum lifetime of 3 months (91 days).

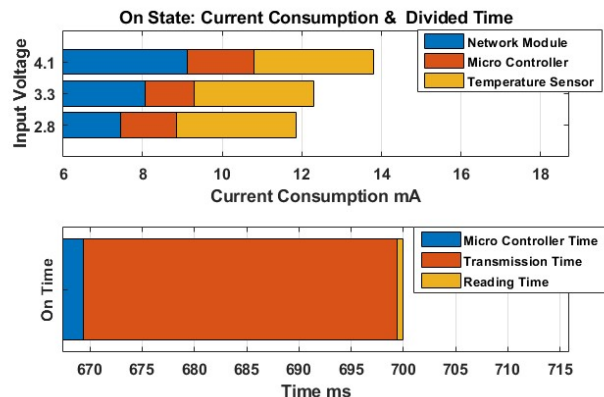


Fig. 19. Bar Graph of the on-state current consumption through each component in the temperature sensor circuit, including the divided time used by each component across the total on time.

This indicated that the circuit optimisation method of a MOSFET disabling the other components during sleep worked and met the design requirement of lasting more than 6 months. Without the addition of the MOSFET, the sleep state current

would have had an additional 453 μ A of measured sleep current from the network module which only provided a maximum lifetime of 5 months.

From Fig. 19, the majority of the current during the on-state was occupied by the network module. The network module's current draw was reducible by lowering its transmit power, with options of 6dbm, 0dbm, -6dbm and -23dbm [24]. Fig. 20 showed that at the lowest transmit power the current consumption reduction only provided an increase in battery life of 9 days. This however significantly reduced the maximum transmission range to 8 meters. It is noted that the network module's current draw in Fig. 19 was based of the 6dbm transmit power, to show the worst-case current consumption.

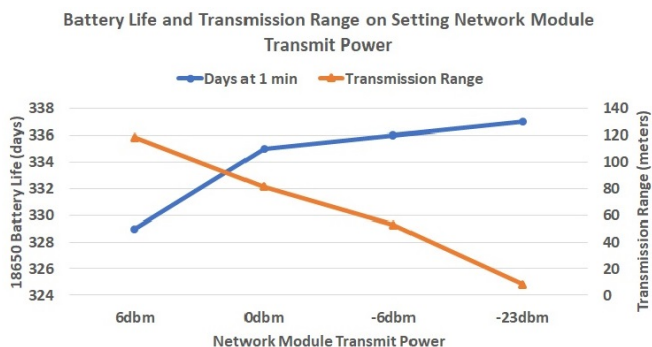


Fig. 20. Line Chart indicating the battery life increase in days versus the received range per transmission power setting.

B. Heat sink & TEG module Performance

The effectiveness of the selected heat sink was assessed by fitting the complete temperature sensor onto a created test rig that simulated the 50 $^{\circ}$ C hot side from the outlet pipe.

Data logging temperature sensors were fitted to the bottom plate of the heat sink and on the hot side of the TEG module. This allowed one to measure the temperature gradient that the TEG module experienced when using the heat sink at the outlet pipe temperatures as seen previously in Fig.3.

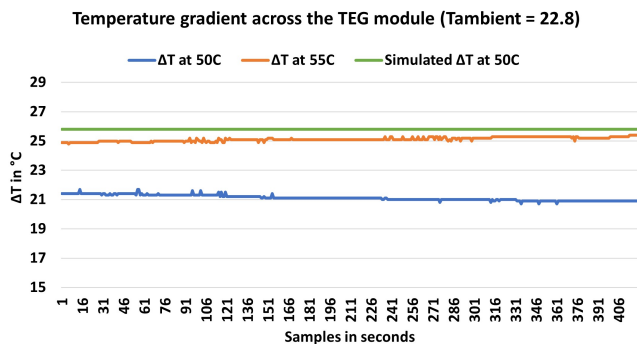


Fig. 21. Temperature gradients across the TEG module relative to hot side temperature

Fig. 21 shows the recorded temperature gradients created by the heat sink. At a hot side temperature of 50 $^{\circ}$ C and 55 $^{\circ}$ C

the temperature gradient formed by the heat sink was above the minimum required temperature gradient of 20 $^{\circ}$ C. The heat sink had therefore met the design requirement of ensuring a maximum cold side temperature of 30 $^{\circ}$ C.

This however was proven otherwise when the corresponding TEG module's open circuit voltage was measured as seen in Fig. 22. The output voltage of 125mV produced by one TEG module was lower than the minimum required input voltage of 225mV for the boost converter. This indicated the boost converter would not operate with a single TEG module. The Seebeck coefficient, α , was recalculated to be 0.005 which was significantly lower than the previously calculated 0.03 in Table 2.

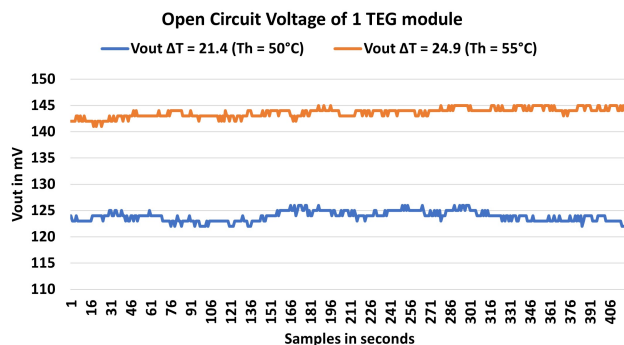


Fig. 22. Open circuit voltage produced by the TEG module using the selected heat sink.

This led to the evaluation of using more TEG modules to produce a higher open circuit voltage. Using two modules in series produced a minimum voltage output of around 300mV which increased to 500mV when using three in series.

The recorded temperature gradients were also compared to the simulated temperature gradient previously found in the thermal conduction analysis, where the simulated temperature gradient was higher, Fig. 21. The cause of the deviation in values could have been due to a higher thermal resistance experienced between touching components.

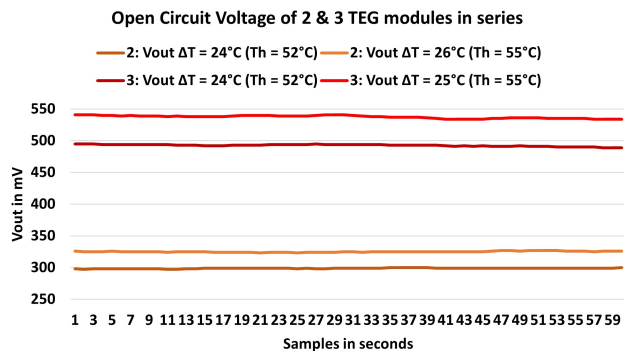


Fig. 23. Combined open circuit voltage of TEG modules in series.

It is noted that by increasing the number of series connected modules, the 3.8 Ω internal resistances of the modules would add therefore slightly lowering total the power output (2) [21]. This links back to the concept of load matching where the

maximum achievable power of the TEG modules was at a load resistance equal to that of their internal resistance (2). Fig. 24 shows a plotted curve of the TEG module’s output power with respect to input voltage at different temperature gradients. This was achieved by using an adjustable resistance box as a load for the TEG module. It is seen that the max power is at points where input voltage had a load equal to that of the internal resistance at 3.8Ω .

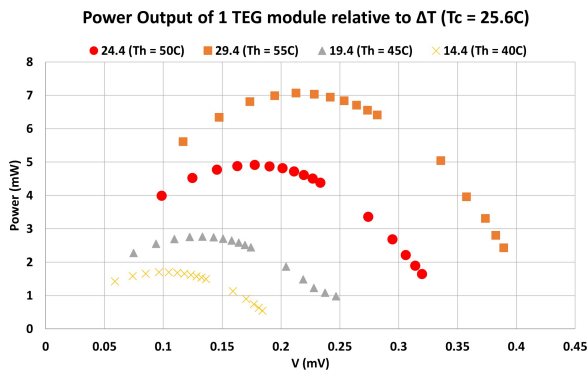


Fig. 24. Power Output of 1 TEG module relative to temperature gradient, showing the maximum power output at load resistance equal to internal resistance.

Using the measured current of the temperature sensor circuit during the on state, the calculated average load resistance of the temperature sensor circuit was 235Ω . At this load resistance the TEG module produced a power output of $360\mu\text{W}$ (2). At 3.3V and at 14mA the total power draw of the temperature sensor circuit was 46.2mW. Comparing the output power and input power required, it shows that the TEG module and boost converter could not directly power the temperature sensor circuit without the battery.

C. Boost Converter & Battery Performance

The performance of the boost converter was evaluated by the minimum input voltage and correlating temperature gradient required to produce a positive current flow towards the battery. This was effectively the point at which the boost converter started to charge the battery. The evaluation also included the efficiency of the boost converter when charging the battery.

The minimum input voltage to the boost converter was acquired by following the temperature growth of the test rig from 23°C to 52°C.

Fig. 25 shows that at 335mV the current flow started to shift towards positive and the input voltage from the TEG modules started a decline to 250mV. At a hot side end point of 52°C, the total current flow towards the battery was 200μA.

The following data gathered for the boost converter experienced a lower temperature gradient than previously experienced in Fig. 25. At 24°C, the small 2°C reduction resulted in 2 TEG modules producing an output voltage of 270mV which was lower than what was needed by the boost converter when connected to the battery.

This is summarised by Fig. 26, where even at 55°C the boost converter topped out at 1.27V with 2 TEG modules in series. This indicated that the system output was temperature sensitive

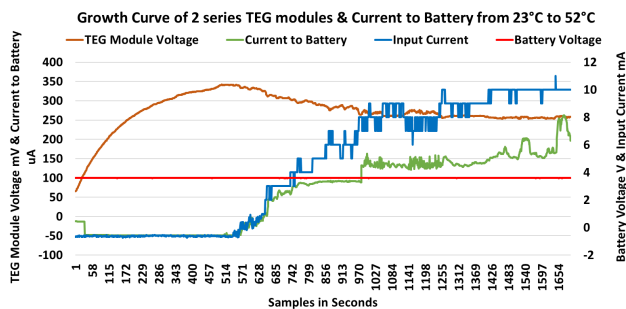


Fig. 25. Input voltage growth to boost converter and resulting output current flow to battery

at 2 modules. This made sense as the open circuit voltage was only 45mV above the required voltage input. Using 3 TEG modules in series ensured a robust setup that provided an output voltage of 4.1V from the boost converter.

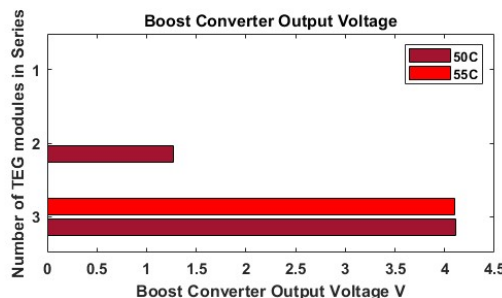


Fig. 26. Measured output voltage of the boost converter, indicating that 2 modules were not enough to produce 4.1V

In Fig. 27, the average boost converter efficiency was 86% at a hot side temperature of 50°C. Not plotted in Fig. 27, the average boost converter efficiency at 55°C hot side temperature was 82% which meant that the boost converter had improved performance at nominal outlet pipe temperature and lower performance when hot water was drawn through the outlet pipe. The input voltage remained at 250mV which was due to the 30kΩ MPPC resistor that limited the input voltage to 300mV [25].

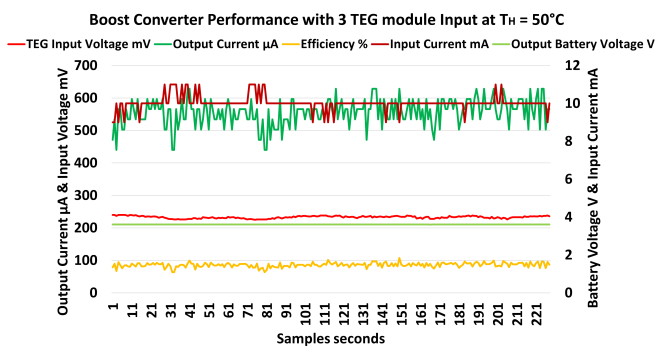


Fig. 27. Boost converter performance with 3 TEG module series voltage input.

When the input voltage is greater than the MPPC voltage, the inductor current is increased until the input voltage is

pulled down to the MPPC voltage [25]. This ensured that more current was fed to the boost converter which resulted in a higher output current to the battery of around 550µA.

A final assessment was performed at the same 225 litre Rheem cylinder where preliminary data was recorded as seen in Fig. 29.

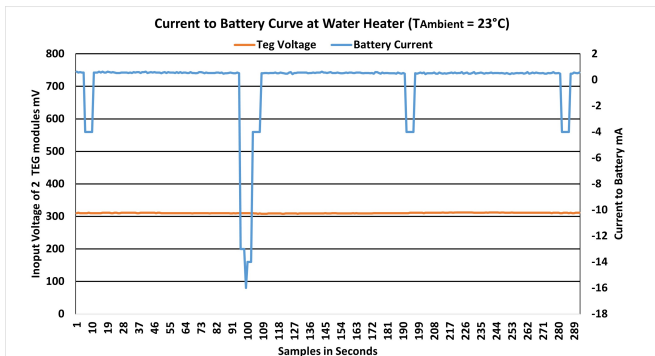


Fig. 28. Current to battery curve at the water heater highlighting the battery current and input voltage from the TEG modules.

Fig. 28 shows a snapshot of the smart temperature sensors performance at a hot side temperature of 50°C from the outlet pipe where the battery current and TEG module voltage was highlighted. Similarly the input voltage was held at around 300mV, which maximised the input current to the boost converter. The battery current had a positive nominal current of 500µA which indicated that the current was flowing towards the battery for charging. The boost converter efficiency resulted in a similar value of 85%.

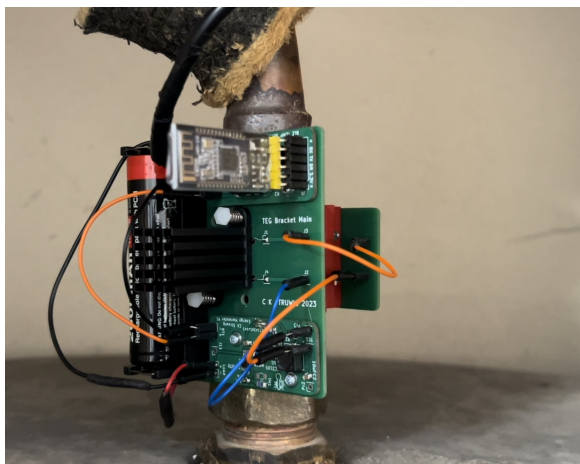


Fig. 29. Image of the smart temperature sensor attached to the outlet pipe of the hot water cylinder.

The negative current spikes in Fig. 28 showed the similar current curve behaviour of the temperature sensor circuit found in Fig. 17. The battery was therefore powering the smart temperature sensor during sampling phases and was charged by the TEG modules through the boost converter during the sleep state. At 500µA current to the battery, a 209µA net positive growth is achieved with respect to the previously found system current consumption of 323µA at 1 minute sample rate. Assuming a 50% battery capacity, the time taken

to charge the battery to 100% was calculated to be over 8 months.

The boost converter and battery evaluation provided the necessary information to indicate that the designed system met the listed design requirements. The boost converter operated at 85% efficiency which met the required conditions of operating in temperatures of 50°C at the hot side and a surrounding 20°C ambient temperature. The average net positive current towards the battery indicated that the smart temperature sensor was able to last indefinitely therefore meeting the minimum required lifetime of 6 months.

D. Cost Analysis

The cost of the smart temperature sensor was evaluated by gathering the total cost of materials and components needed to produce the device. Table 3 shows the summarised list of required components and materials. The total cost for the smart temperature sensor is \$212 which is lower than the \$300 average for ripple control relays, therefore meeting the design requirement of being a more affordable alternative to ripple control [7]. The temperature sensor however is not complete without the hot water controller. To truly meet being more affordable than the ripple control relay, the hot water controller has to developed with the cost constraint of \$82.

TABLE III
SUMMARISED LIST OF NEEDED COMPONENTS FOR THE SMART TEMPERATURE SENSOR [21]–[26], [28]

Components	Description	Cost
Battery	2600mAh Li-ion Battery	\$32
TEG Modules	NL1023T Thermoelectric Generator	\$68
Heat sink	19x33mm Push Pin Heat sink	\$11
Circ. Components	LTC3105, LTC4070 & AT-TINY 85	\$23
Temp. Sensor	DS18B20 IC Temperature Sensor	\$13
Network Module	HM-10 BLE Network Module	\$39
PCB	Boost Converter & Temperature Sensor	\$25

The smart temperature sensor was developed with three separate PCBs which can be merged into a single PCB in future development, which would reduce the cost to \$195. The calculated total cost is with respect to using 2 TEG modules and would increase by \$40 if an additional module was required.

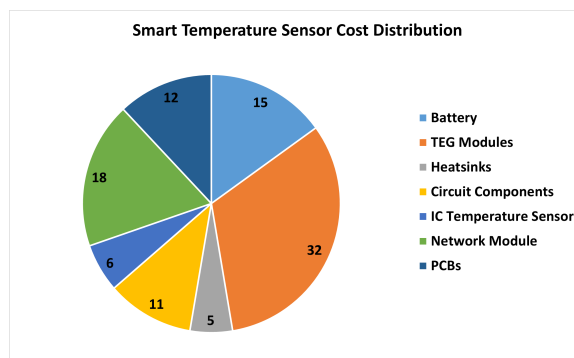


Fig. 30. Pie chart showing the component contribution percentage relative to the total cost

Fig. 29 shows that the largest contributors are the TEG modules which is \$34.27 for each module. It is shown that 51% of the total cost was from harvesting the available thermal energy, by including the boost converter circuit and heat sink percentages.

If the temperature sensor circuit was only supplied by the battery the total cost is reduced to \$95. This highlights that a purely battery powered system would be more cost effective, this however requires that the battery is replaced after 10 months assuming a full battery at a 1 minute sampling rate.

VI. CONCLUSION AND FUTURE WORK

A. Future Work

The development of the smart temperature sensor allows for the future project goal of developing a hot water controller. The hot water controller is a power control circuit that manages the AC power fed to a hot water cylinder by means of pulse width modulation. The amount of power fed to the hot water cylinder is based on a received control signal.

The control signal for the hot water controller would be the wireless temperature reading received from the smart temperature sensor. Pulse width modulation of an alternating current wave would require switching components that allow for bidirectional current flow such as a Bidirectional triode thyristor or TRIAC. This would also require the design of a feedback controller that adjusts its output proportionally to the temperature readings received from the smart temperature sensor.

The smart temperature sensor could be improved in future work by developing code on the microcontroller that would dynamically reduce the sampling rate, lowering the systems average current consumption, depending on the hot side temperature detected by the temperature sensor.

The microcontroller uses the temperature gradient to calculate the expected input voltage from the TEG modules by using their stored Seebeck coefficients (1). This would then allow for the controller to determine the resulting input current and adjust the sampling rate accordingly. This ensures that the current consumption is always lower than input current, continuously charging the battery at lower temperatures.

B. Conclusion

In conclusion, the development and evaluation of the smart temperature sensor represent a significant step toward the utilization of waste heat energy in various applications. This device successfully captures thermal energy and converts it into usable electrical power for sustainable operation.

The project demonstrates an innovative approach to energy harvesting, specifically using a thermoelectric generator (TEG) in conjunction with a boost converter to power a wireless temperature sensor. Through testing and evaluation, the system showed good performance, meeting or exceeding the design requirements in several key aspects.

The heat sink and TEG module performance, as well as the efficiency of the boost converter, were critical to the success of the system. The heat sink effectively managed the minimum temperature gradients across the TEG module, meeting the

necessary requirements for energy conversion. By using three TEG modules in series, the system was able to generate a robust output voltage for the boost converter, ensuring consistent power generation across a range of temperatures.

With careful power management, the device can operate indefinitely, recharging its battery from the harvested thermal energy. The cost analysis also indicated that the system is economically viable, making it a suitable alternative to demand management systems like ripple control relays.

Its innovative approach, efficiency, and cost-effectiveness position it as a promising technology for sustainable energy management, paving the way for future advancements in the domain of waste heat utilization.

VII. REFERENCES

REFERENCES

- [1] Markets Team. *Energy in New Zealand 2023*. Ministry of Business, Innovation and Employment, Wellington, New Zealand, 2023.
- [2] Tyler Byers Nicola Burroughs, Kate Kolich and Viktoria Nordstrom. *Electric Vehicle Charging Survey - Insights into EV owners' charging habits, and use of public EV charging*. Energy Efficiency & Conservation Authority (EECA), Wellington, New Zealand, 10 2021.
- [3] Ministry of Transport. Land transport act 1998: Section 167c (clean vehicle standard). Technical Report SL 2022/285, Parliamentary Counsel Office, 2022.
- [4] Jun Su, T.T. Lie, and Ramon Zamora. Modelling of large-scale electric vehicles charging demand: A new zealand case study. *Electric Power Systems Research*, 167:171–182, 2019.
- [5] Neville Watson, Jeremy Watson, Russell Watson, Kashani Sharma, and Allan Miller. Impact of electric vehicle chargers on a low voltage distribution system. 06 2015.
- [6] New Zealand Treasury. Electricity demand-side management. *Research and commentary*, 2007.
- [7] Energy Efficiency & Conservation Authority. *Ripple Control of Hot Water in New Zealand*. New Zealand Government, 2020.
- [8] Jose Antonio Barros Vieira and Alexandre Manuel Mota. Thermoelectric generator using water gas heater energy for battery charging. In *2009 IEEE Control Applications, (CCA) & Intelligent Control, (ISIC)*, pages 1477–1482, 2009.
- [9] Matthew Dargusch et al. Thermoelectric generators: Alternative power supply for wearable electrocardiographic systems. *Applied Science*, 7:264–287, 2020.
- [10] Nesrine Jaziri, Ayda Boughamoura, Jens Müller, Brahim Mezghani, Fares Tounsi, and Mohammed Ismail. A comprehensive review of thermoelectric generators: Technologies and common applications. *Energy Reports*, 6:264–287, 2020. SI:Energy Storage - driving towards a clean energy future.
- [11] Yuming Liu, Jordi-Roger Riba, Manuel Moreno-Eguilaz, and Josep Sanllehi. Application of thermoelectric generators for low-temperature-gradient energy harvesting. *Applied Sciences*, 13(4), 2023.
- [12] Alfred Smith. How thermoelectric generators work.
- [13] Wervyan Shalannanda, Irma Zakia, Erwin Sutanto, and Fahmi Fahmi. Design of hardware module of iot-based infant incubator monitoring system. In *2020 6th International Conference on Wireless and Telematics (ICWT)*, pages 1–6, 2020.
- [14] Layal Esmael and Their Ibrahim. Design of a real time wireless data acquisition system for control purposes. *International Journal of Computer Applications*, 177:27–33, 12 2019.
- [15] Selçuk Yazar, Deniz Taşkın, and Cem Taşkın. Developing a bluetooth low energy sensor node for greenhouse in precision agriculture as internet of things application. *Advances in Science and Technology Research Journal*, 12, 12 2018.
- [16] Cuong M. Nguyen, Jeffrey Mays, Dakota Plesa, Smitha Rao, Minh Nguyen, and J.-C. Chiao. Wireless sensor nodes for environmental monitoring in internet of things. In *2015 IEEE MTT-S International Microwave Symposium*, pages 1–4, 2015.
- [17] 1983 Standards Council. Copper tubes for water, gas, and sanitation. Technical Report NZS-3501-1976-A1, Standards Association of New Zealand, Wellington Trade Center, Wellington, 1976.
- [18] Marlow Industries. *Technical data sheet for RC3-2.5*, 2002. Rev. F.
- [19] Marlow Industries. *Technical data sheet for RC3-4*, 2002. Rev. L.

- [20] Marlow Industries. *Technical data sheet for RC6-4*, 2002. Rev. N.
- [21] Marlow Industries. *Technical data sheet for NL1023T*, 2002. Rev. L.
- [22] Atmel. *Atmel 8-bit AVR Microcontroller with 2/4/8K Bytes In-System Programmable Flash*, 2013. Rev. 2586QS.
- [23] Maxim Integrated. *Programmable Resolution 1-Wire Digital Thermometer*, 2017. Rev. 6.
- [24] Sihai Corp. *HM-10 Datasheet*, 2017. Ver. 545.
- [25] Linear Technology. *400mA Step-Up DC/DC Converter with Maximum Power Point Control and 250mV Start-Up*, 2012. Rev. 3105fb.
- [26] Linear Technology. *Li-Ion/Polymer Shunt Battery Charger System*, 2012. Rev. D.
- [27] Ultimaker ABS. *Technical Datasheet on ABS*, 2017. Version 3.006.
- [28] Wakefield-Vette. *Wakefield-Vette 960 Series Push Pin Heat Sink*, 1999. Rev. C.